Phase measuring deflectometry based microscopy for shape visualization and thickness quantification

Sharma, Shivam; Trivedi, Vismay; Mahajan, Swapnil; Sheoran, Gyanendra; Javidi, Bahram; Anand, Arun

DOI
10.1016/j.optlastec.2025.113524

Publication date
2025

Document Version
Final published version

Published in
Optics and Laser Technology

Citation (APA)
Sharma, S., Trivedi, V., Mahajan, S., Sheoran, G., Javidi, B., & Anand, A. (2025). Phase measuring deflectometry based microscopy for shape visualization and thickness quantification. *Optics and Laser Technology*, *192*, Article 113524. https://doi.org/10.1016/j.optlastec.2025.113524

Optics & Laser Technology 192 (2025) 113524

Contents lists available at ScienceDirect

Optics and Laser Technology

journal homepage: www.elsevier.com/locate/optlastec

Full length article

Phase measuring deflectometry based microscopy for shape visualization and thickness quantification

Shivam Sharma [a,1], Vismay Trivedi [a,b,1,*], Swapnil Mahajan [c], Gyanendra Sheoran [a], Bahram Javidi [d], Arun Anand [e]

[a] Advanced Research in Optical and Microwave Applications (AROMA) Lab, Department of Applied Sciences, National Institute of Technology (NIT), Delhi 110036, India
[b] Department of Aerospace Structures and Materials, Delft University of Technology, Kluyverweg 1, 2629 HS Delft, the Netherlands
[c] Applied Physics Department, Faculty of Technology and Engineering, The M S University of Baroda, Vadodara, India
[d] Department of Electrical and Computer Engineering, University of Connecticut, Storrs, CT 06269-4157, USA
[e] Optics Laboratory, Department of Physics, Sardar Patel University, Vallabh Vidyanagar, Anand 388120, India

ARTICLE INFO

Keywords:
Quantitative phase contrast imaging
Phase measuring deflectometry
Fringe pattern analysis
Thickness measurement
Shape profiling

ABSTRACT

Shape profiling and thickness information of living cells can provide critical insights about the cells, which can help in their identification and characterization. Most living cells are difficult to image as they are very small and almost transparent. In conventional bright-field microscopy, this issue is resolved by using staining agents, but they can potentially disrupt a cell's natural life cycle. Generally, to address this issue, quantitative phase contrast imaging, such as digital holography is employed, as it provides direct phase information. However, in some practical applications, employing the digital holography technique can become challenging due to stringent optical requirements and its high sensitivity to thickness change. Here, we present phase measuring deflectometry as a microscopy technique by employing a four-step phase-shifting method for shape visualization and thickness measurement of transparent micro-objects. The technique provides phase that is proportional to the deflection angle, which, in turn, depends on the gradient of the optical thickness of the sample. So, the system was calibrated using a 5 μm diameter transparent polystyrene microsphere. A scaling factor was determined by the calibration process, which was then tested by measuring the thickness of a 15 μm diameter transparent polystyrene microsphere. This result obtained with phase measuring deflectometry agrees with the digital holographic microscopy measurement. The proposed technique was further used for visualization and thickness measurement of the red blood cells (RBCs). Based on the available information, the presented technique and algorithm have not been previously exploited for shape visualization and thickness measurement of transparent micro-objects.

1. Introduction

The morphological, chemical, and mechanical parameters, and the cell count, can serve as indicators of an individual's health [1]. So, quantifying such parameters can help in cell classification and disease diagnosis. Increased demand for inspecting and characterizing cells has led to the development of various microscopy techniques and modalities [2,3]. Most microscopy methods rely on detecting the intensity and colour of light generated by the interaction between the illuminating field and the sample being examined. Conversely, the cells tend to be transparent since it does not appreciably change the amplitude of the electromagnetic radiation (specifically visible radiation) interacting with them [2]. So, amplitude-contrast imaging of such specimens becomes very difficult. Enhancing contrast often involves chemical dyes, leading to staining artifacts [4,5]. Furthermore, the processing of chemical labelling and staining of the cell can terminate or alter the cell's life cycle. Therefore, this additional step of chemical exposure is not ideal for characterizing live cells in their natural physiological state.

An approach to addressing this challenge is by capturing the phase of the probe beam. Quantitative phase contrast imaging (QPI), a label-free

* Corresponding author at: Advanced Research in Optical and Microwave Applications (AROMA) Lab, Department of Applied Sciences, National Institute of Technology (NIT), Delhi 110036, India.
E-mail address: vismay.trivedi@gmail.com (V. Trivedi).
[1] The authors contributed equally to this work.

https://doi.org/10.1016/j.optlastec.2025.113524
Received 18 January 2025; Received in revised form 4 June 2025; Accepted 4 July 2025
Available online 7 July 2025

technique, addresses the aforementioned issue by measuring nanometer-scale phase changes [6]. One of the most commonly used approaches to performing QPI is using Digital Holography, which can directly and non-invasively provide phase information [7,8]. Different geometries have been employed over the past few decades for various QPI related applications in microscopy, surface profiling, shape measurement, thermal mapping, and defect detection [9–22]. Although digital holography has been extensively utilized for various microscopy applications, its practical applications can be constrained due to cumbersome procedures, its limitations for measurement over a small thickness range, and other stringent requirements and equipment [10]. Thus, this technique is effective for thin or weak phase objects and not for objects possessing significant thickness.

An uncomplicated, cost-effective method with a larger range of measurements that can produce quantitative phase-contrast images can be advantageous. One such method is phase measuring deflectometry (PMD). In the case of PMD, the screen displaying the fringe pattern needs to be imaged through the object of interest [23–26]. Conversely, for objects with specularly reflecting surfaces, the fringe pattern must be imaged upon reflection from the shiny surface [27]. For transparent objects, due to the variation in optical thickness, the light passing through the object refracts, which causes the fringe pattern to get modulated. The modulation in the fringe pattern can be digitally recorded and numerically processed with a well-developed fringe analysis algorithm to obtain phase information [28,29].

In this article, we endeavor to explore the PMD technique for microscopy applications using a four-step phase-shifting method. Demonstrating the ability of the proposed technique for shape visualization and to compute the thickness of the transparent micro-objects were the prime objectives of the work. The present work is a proof-of-concept experiment where the proposed technique has a simplistic design with a smartphone screen used for displaying the fringe pattern, making the microscopy system simple and cost-effective.

In this article, we explore the application of PMD to microscopy using a four-step phase-shifting method. The primary objective of this proof-of-concept study is to demonstrate the feasibility of PMD for shape visualization and thickness measurement of transparent micro-objects. The proposed setup employs a simplified design featuring a demagnified fringe pattern displayed on a smartphone screen, making the system compact, accessible, and cost-effective.

Although PMD has traditionally been applied in reflective-surface metrology, its extension to transparent biological samples remains largely unexplored. This approach could be confused with Structured Illumination Microscopy (SIM), which was originally developed to reject out-of-focus light and later adapted for super-resolution fluorescence imaging. SIM uses phase-shifted grid patterns at various orientations to generate moiré fringes that enable sub-diffraction-limit resolution through computational reconstruction [30–32]. In contrast, our PMD-based technique does not intend to enhance resolution but instead performs quantitative phase contrast imaging. A sinusoidal fringe pattern is imaged through the sample, and local variations in optical thickness modulate this pattern due to refraction. The resulting phase shifts, calculated using a four-step phase-shifting algorithm, correspond to the gradient of optical thickness perpendicular to the fringe orientation. In summary, SIM recovers high-resolution spatial detail through fluorescence modulation, while PMD measures optical-path-length distributions to quantify shape and thickness using simple, incoherent illumination.

2. Theoretical background

The fundamental principle of PMD in the transmission mode is the law of refraction, where any change in the optical path length leads to the bending of light rays towards the regions of higher optical path length [33]. This bending of light rays can be quantified by computing the change in the image of the fringe pattern recorded by placing the object of interest between the fringe pattern and the imaging system (a combination of a lens and a digital array such as a CCD and CMOS) [25]. Since the technique relies on the change in optical path lengths, it could only provide a phase (that is proportional to the angle of bending/deflection) in terms of the gradient of the optical thickness perpendicular to the direction of fringe orientation. Thus, to obtain the actual value of the optical thickness, the phase needs to be integrated along the length of the sample in both directions perpendicular to the light propagation direction [34].

To extract phase information encoded in the fringe pattern, various fringe analysis algorithms are employed [35]. Due to its simplicity and effectiveness, the Fourier Transform-based fringe analysis is a widely used algorithm in optical metrology, particularly for phase measurement. However, achieving sufficient fringe density is crucial for its effective implementation [36,37]. Since ensuring adequate fringe density across micro-objects is essential for the efficient extraction of phase information using the Fourier transform, demagnifying the displayed fringe pattern to a sufficient level became necessary. Moreover, demagnifying the fringe pattern to such an extent became very challenging. Thus, a four-step phase shifting method [38] was employed to compute the phase of the probe beam interacting with the micro-objects. The four-step approach is widely used due to its inherent ability to suppress harmonics and mitigate errors caused by imperfect system calibration or environmental factors. It ensures complete phase determination with good noise immunity, which is critical for the reliability and reproducibility of the technique presented here [38,39].

The numerically processed images provide the required phase, which, upon integration along individual directions, gives the optical thickness values for those directions. The process of excessing the phase information of a transparent object using PMD and four-step phase shifting is described below.

Assuming a sinusoidal fringe pattern extending across the *x*-*y* plane with spatial variation in the *y* direction (Horizontal Fringe Pattern- to extract information in *y* direction), was displayed on a digital screen as shown in Fig. 1, which was imaged and recorded using an imaging system consisting of a lens and a digital array.

In the proposed approach, the image of the fringe pattern after passing through the medium surrounding the micro-object acts as a reference. To apply the four-step phase shifting algorithm, four phase-shifted fringe patterns with a shift of $(\pi/2)$ are sequentially displayed on the digital screen and subsequently recorded by the imaging system. Let the equation describing the recorded intensity distribution associated with the reference image $I_{ref(h)}(x, y)$ (unmodulated fringe pattern) be [40]

$$I_{ref(h)}(x,y) = I_0 + I\cos\left(\frac{2\pi y}{p} + \phi\right) \tag{1}$$

where, I_O represents average background intensity, I represent intensity modulation term, p is the fringe width and $\phi = 0, \pi/2, \pi, 3\pi/2$. Now,

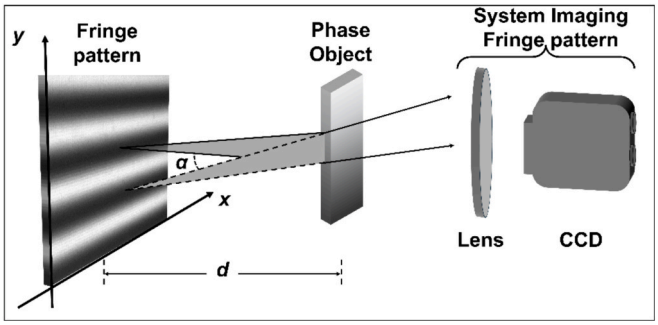

Fig. 1. Phase deflectometry in one dimension: Fringe pattern displayed on the screen of a smartphone and fringe shift at angle α due to phase object placed at a distance d from the screen.

when a transparent phase object (in our case micro-objects with the surrounding medium like transparent polystyrene beads in oil and red blood cells (RBCs) in blood plasma) was introduced between the displayed fringe system and the imaging system, due to the change in the optical path length experienced by the light beam while passing through the object, the image of the fringe pattern gets deflected which leads to the modulation of the original fringe pattern. The angle of deflection of the light beam is $\alpha \approx (\partial S(x,y)/\partial y)$, where $S(x, y)$ is the optical path length accumulated by the light beam passing through the phase object at position (x, y). If d is the distance between the fringe pattern and the object, the fringe shifts in the y direction by distance $\alpha d \approx d(\partial S(x,y)/\partial y)$ [40]. So, the phase associated with the numerically processed fringe pattern is proportional to the deflection angle α. Thus, it can be inferred that the gradient of optical thickness is proportional to the phase, which in turn is proportional to the deflection angle. The intensity distribution of the recorded four-step phase shifted fringe patterns seen through the object with the surrounding medium can be described as [40]

$$I_{obj(h)}(x,y) = I_0 + I\cos\left(\frac{2\pi y}{p} + \frac{2\pi d}{p}\frac{\partial S(x,y)}{\partial y} + \phi\right) \tag{2}$$

Similarly, images are obtained for a sinusoidal fringe pattern extending across the x-y plane with spatial variation in the x direction (Vertical Fringe Pattern- to extract information in x direction) is displayed on a digital screen. For each set of fringe pattern (Horizontal and Vertical), 4 fringe patterns associated with a reference and 4 fringe patterns associated with an object are recorded. So, a total of 16 fringe patterns are recorded for extracting phase information from a single field of view as shown in Fig. 2.

After applying four-step phase shifting algorithm to these recorded images, wrapped phase for the object, and references for each fringe orientation are obtained. These wrapped phases are unwrapped using a 2D fast Fourier transform unwrapping algorithm [41] to get continuous phase distributions $\phi_{ref(H)}$ and $\phi_{obj(H)}$ associated with reference and object respectively. The continuous phase difference (ϕ_H) obtained using the horizontal fringe system is given by

$$\phi_H = \phi_{obj(H)} - \phi_{ref(H)} = \frac{2\pi d}{p}\frac{\partial S}{\partial y} \Rightarrow \phi_H \propto \frac{\partial S}{\partial y} \tag{3}$$

Similarly, the continuous phase difference (ϕ_V) associated with vertical fringe pattern is also computed.

$$\phi_V = \phi_{obj(V)} - \phi_{ref(V)} = \frac{2\pi d}{p}\frac{\partial S}{\partial x} \Rightarrow \phi_V \propto \frac{\partial S}{\partial x} \tag{4}$$

It can be seen from Eq. (3) and Eq. (4) that the phase values for the horizontal and vertical fringe patterns are proportional to the gradient of optical path length along y and x directions respectively. Now, taking partial derivative of ϕ_H with respect to y and ϕ_V with respect to x and adding them results in the Poisson's equations as follows:

$$\left(\frac{2\pi d}{p}\frac{\partial^2 S}{\partial x^2}\right) + \left(\frac{2\pi d}{p}\frac{\partial^2 S}{\partial y^2}\right) = K\left[\frac{\partial^2 S}{\partial x^2} + \frac{\partial^2 S}{\partial y^2}\right] = K[\nabla^2 S] \tag{5}$$

where $K = \frac{2\pi d}{p}$ .The solution of Eq. (5) gives the product of the optical path length $S(x, y)$ and a scaling factor K. A detailed discussion regarding the solution of Poisson's equation is provided by J.L. Flores et al.[40], where the primary focus was on developing a method for analyzing fringe patterns of orthogonal nature, while the present work focuses on the development and application of PMD as a quantitative phase contrast microscopy technique for imaging phase micro-objects, including red blood cells.

To summarize the process of thickness measurement through PMD, a flow chart describing individual steps is shown in Fig. 3. The scaling factor K in Eq. (1) was computed from a sample with known optical thickness and was subsequently used for shape profiling and optical thickness measurement for samples with unknown thickness or refractive index difference.

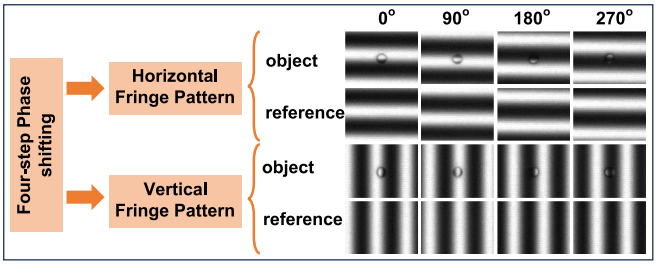

Fig. 2. Recorded four-step Phase shifting for horizontal as well as vertical fringe patterns.

3. Experimental setup

Fig. 4(a) and (b) show the table-top experimental and schematic of the experimental setup employed for shape visualization and thickness measurement of transparent micro-objects. Sinusoidal fringe patterns with phase-shifted images were sequentially displayed on the screen (brightness: 800 nits) of a smartphone. The smartphone display is chosen for its flexibility in dynamically generating and updating fringe patterns, with software-based control over parameters such as pitch, orientation, and phase shifts. This eliminates the need for physical gratings or mechanical adjustments. Its compact size, fine pixel resolution, and brightness make it a convenient and adaptable tool for compact optical setups. These patterns are demagnified using a condenser lens (MO1:100 × , NA = 1.25 oil immersion) operated in dry mode kept 14 cm from the display screen. The pitch of the fringe patterns at the image plane of MO1 turns is 6.45 μm. This demagnified image serves as the probe fringe pattern for the imaging lens (MO2: 20 × , NA = 0.40). The magnified image of this fringe system projected through the test object is recorded with a CCD array (ThorLabs DCU223M, 8-bit, 4.65 μm pixel pitch), which was placed 19 cm from MO2 (20X DIN Achromatic Finite conjugate). The sample plane was located just above the image plane of MO1 (at a distance d from the image plane). The object modulated the fringe pattern due to spatially varying optical thickness. The phase from the numerically processed image is the measure of the deflection of the fringe pattern, which in turn was proportional to the gradient of the optical thickness and was quantified using the four-step phase shifting method. Although MO1 is an oil immersion objective, it was operated in dry mode for this proof-of-concept experiment to simplify the setup. While this reduces the effective NA and introduces potential aberrations, calibration measures were implemented to capture and minimize baseline phase errors. A reference phase was computed to account for systematic phase deviations.

As this is a proof-of-concept experiment aimed at demonstrating the effectiveness of the PMD technique for measuring and mapping the optical thickness of transparent micro-objects, parameters of the smartphone display, such as pixel pitch and brightness, are not examined in detail. Instead, the system is calibrated to eliminate baseline phase errors or noise potentially introduced by the display's protective structures, which may cause diffractive and refractive effects. To establish this baseline, a reference frame is captured prior to each measurement, which captures any phase deviations due to the display alone. Consequently, by detecting only the relative phase changes between the reference and object frames, the system effectively neutralizes such artifacts due to the display screen.

4. Results and discussion

Initially, the system's magnification is computed by imaging a USAF resolution target (Thorlabs R1DS1N), yielding a magnification factor of 24.35. Since the phase derived from the proposed technique is directly proportional to the gradient of optical thickness, the system's calibration involves using a sample of known thickness immersed in a known

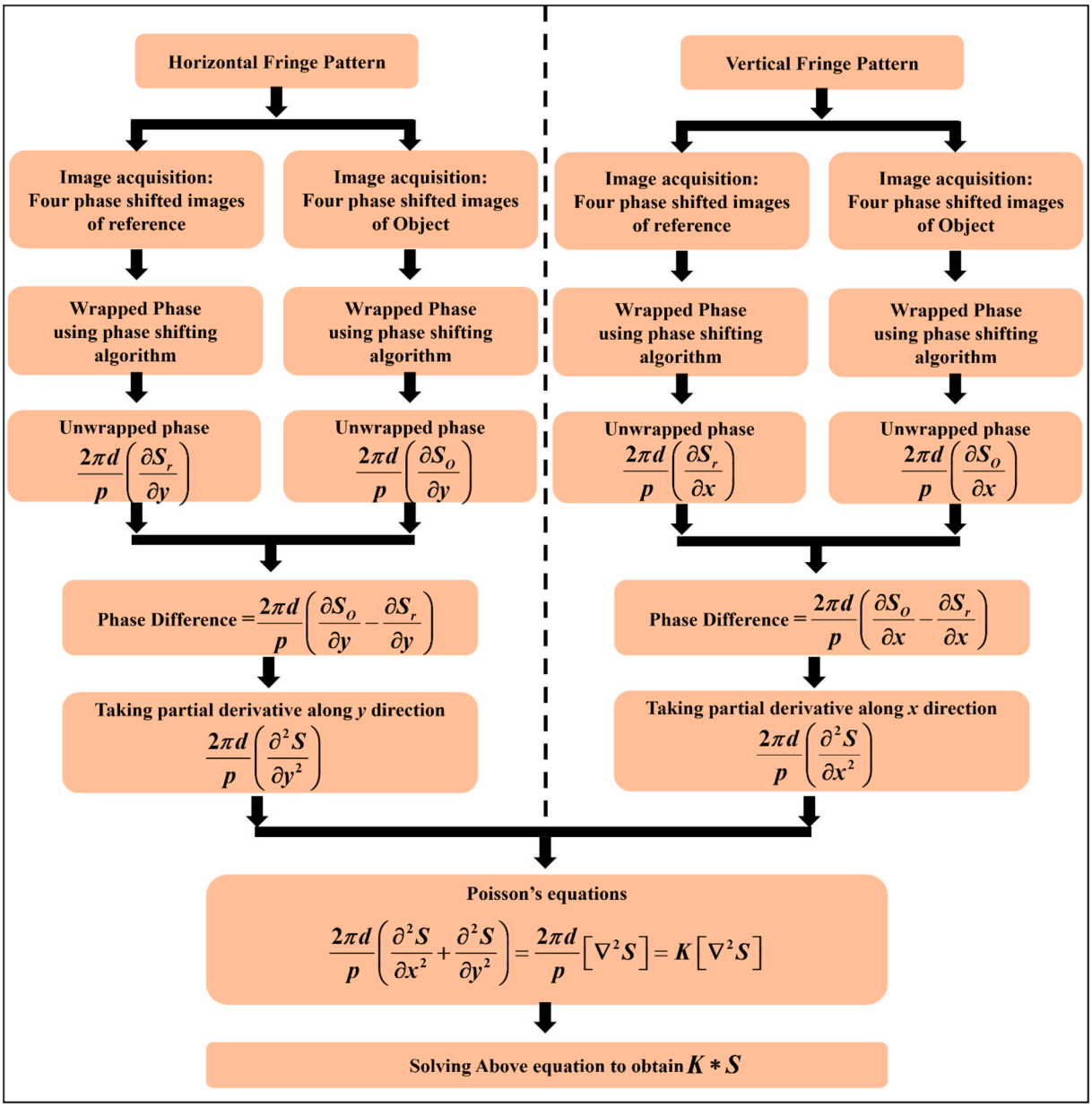

Fig. 3. The process of computing optical path length travelled by the light beam while passing through the sample.

medium (known refractive index difference). This calibration establishes a correlation between phase and optical thickness, enabling accurate thickness measurements of subsequent test samples.

To demonstrate the versatility of the proposed technique, optical thickness measurements were performed on three different types of samples. After calibrating the system with a transparent polystyrene micro-sphere of a specific diameter, the technique was applied to measure the optical thicknesses of another transparent polystyrene microsphere with a different diameter, RBCs, and pollen seeds.

The initial set of experiments involved imaging transparent polystyrene micro-spheres (refractive index of 1.58) of a known diameter of 5 ± 0.8 μm (SPI Supplies), which were immersed in microscope immersion oil (refractive index of 1.52). The four-step phase shifting method was applied with two different fringe orientations: horizontal and vertical fringe patterns to compute the scaling factor *K*.

Fig. 5 illustrates the results obtained during the calibration of the developed microscopy system. Fig. 5(a) and (b) depict the unwrapped phase differences obtained between the object and reference images, associated with the horizontal and vertical fringe patterns, respectively. Then, the partial derivatives of Fig. 5(a) and (b) were calculated and added to obtain their second derivatives, giving rise to Eq. (5) (Poisson's Equation). Finally, the integrated phase of the microsphere was obtained by computing the solution of Eq. (5) and is shown in the Fig. 5(c). Fig. 5 (d) and (e) represent the 3D rendering and the line profile of the thickness (along the line shown in Fig. 5(c)). Since the thickness and the refractive index difference (with the surrounding medium) of the sample are known, they were used to obtain the scaling factor *K* from the phase distributions. The value of the scaling factor *K* was computed, which turns out to be 23.33 ± 2.23/μm. The standard deviation in the *K* values is about 9 %, which includes the standard deviation of 7.6 % in size of the microspheres provided by the manufacturer and is the measurement error of the proposed microscopy system. This value of scaling factor *K* was utilized for the thickness measurement of unknown samples with known refractive index differences. So, the protocol for determination of the scaling factor K includes (i) recording of the projected pattern using an object with known thickness and diameter (calibrating object), (ii) recording of the pattern projected through the medium surrounding the calibrating object, (iii) Phase difference computation using the

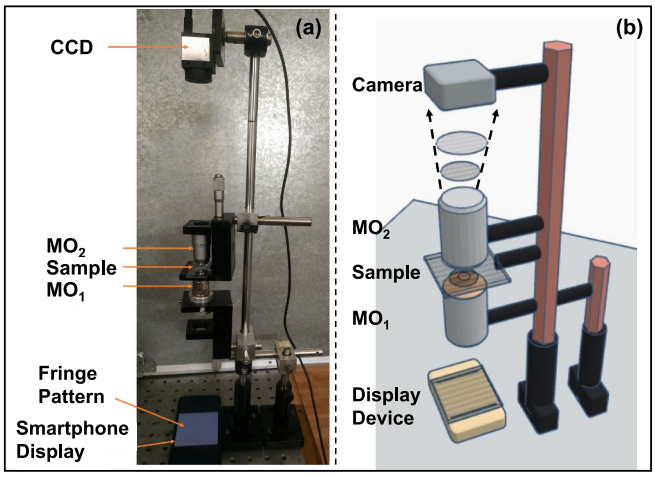

Fig. 4. Experimental Setup (a) Table-top version (b) Schematic.

algorithm shown in Fig. 3 and (iv) Computation of K from the thickness and refractive index values of the calibrating sample. Since the technique relies on quantifying the bending of light caused by the refractive index difference between the object and its background, a larger difference in refractive index between the sample and the surrounding medium results in more pronounced bending of the projected pattern for the same object, influencing the calibration accuracy of PMD. When the refractive index difference is higher, the bending of light becomes significantly more pronounced, which in some cases, leads to overlapping or merging of the projected pattern, resulting in phase errors during measurement. Such errors can affect the accuracy of the phase map and calibration. Furthermore, the use of immersion oil creates a uniform and homogeneous surrounding medium, ensuring consistent light propagation through and around the object under investigation. This homogeneity is particularly important for accurate calibration, especially when working with non-flat samples like microspheres.

The value of the computed scaling factor K was verified by applying it to measure the thickness of a transparent polystyrene microsphere of diameter 15 ± 0.9 μm immersed in microscope oil. It can be seen from Fig. 6 that the average value of K was effectively utilized in shape profiling and thickness measurement. Fig. 6(a), (b), and (c) represent the continuous phase distribution, 3D rendering of the thickness, and line profile of the thickness (along the line shown in Fig. 6(a)). The thickness of the microsphere calculated using the computed K is 15.46 ± 0.75 μm. This thickness value falls within the standard deviation as specified by the manufacturer.

To further validate the system's ability to measure thickness, the microsphere of diameter 15 ± 0.9 μm (of the same specifications as measured with PMD) was measured using an already developed digital holographic microscope (DHM) based on Mach Zehnder geometry [42]. The DHM results shown in Fig. 6 utilize a similar system design and configuration as described in reference 38. The microsphere measurements presented (15 ± 0.9 μm) were conducted specifically for this study and are not part of the reference 38. The thickness of the microsphere obtained using this approach is 15.3 μm. The results obtained from DH microscopy validate the efficiency of the proposed PMD-based microscope, as shown in Fig. 6(d)–(f). In addition to providing comparable results, the PMD-based setup offers several practical advantages over digital holographic microscopy (DHM). The use of an incoherent fringe source avoids speckle noise and parasitic reflections commonly associated with coherent laser illumination in DHM. Moreover, PMD does not rely on interference between separate optical paths, making it inherently less sensitive to environmental vibrations and alignment errors. The optical arrangement is also simpler, using fewer precise components and requiring less stringent alignment. These features make PMD a robust and cost-effective alternative for scenarios where DHM may be limited by coherence-related noise, sensitivity to mechanical instability, or setup complexity. Although the measurements obtained using PMD and DHM match, it could be deduced from Fig. 5 and Fig. 6 that the phase stability associated with PMD is lower than that obtained by DHM. Since the PMD technique provides optical thickness from deflection information of the probe beam using a four-step phase shifting algorithm which is used for interferometric techniques, it led to lower spatial phase stability. Also, PMD involves numerical integration of the obtained gradient of optical path length distribution, which leads to the submerging of high spatial frequency structures. The standard deviation of the background phase acts as the longitudinal measurement accuracy of the technique and is around 9.6 nm which is computed after

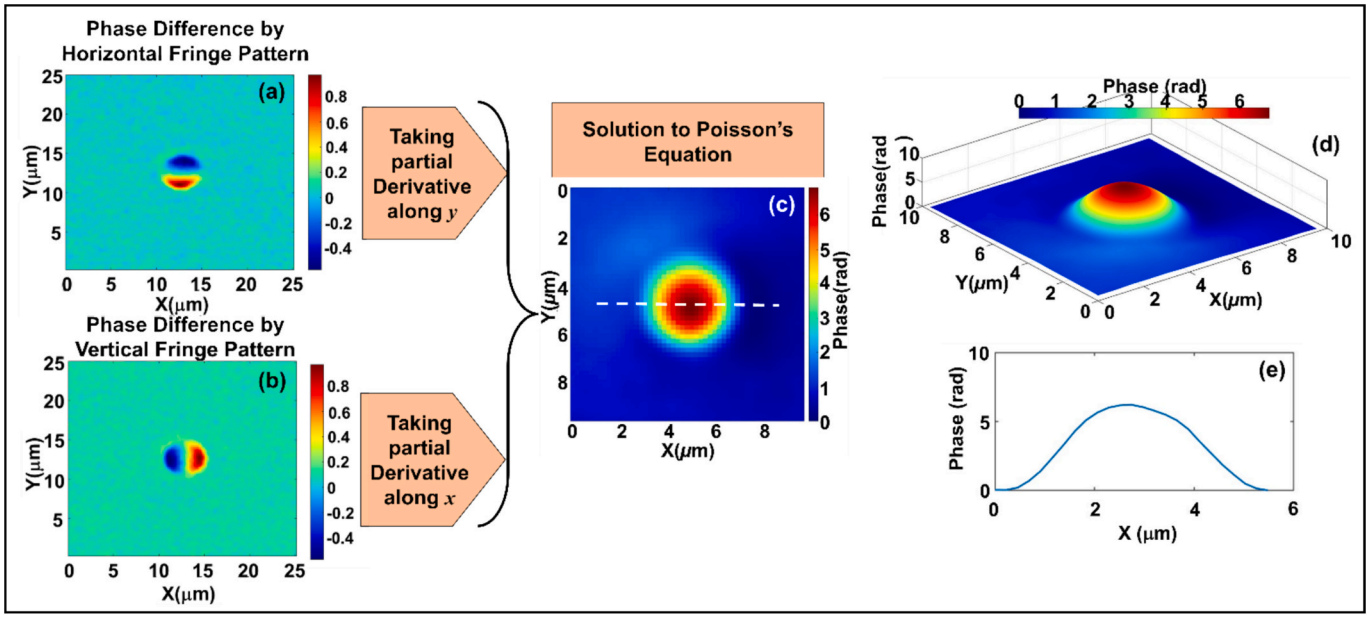

Fig. 5. Calibration using transparent polystyrene microspheres of 5 μm diameter (a) and (b) are unwrapped phase differences obtained using horizontal and vertical fringe patterns (c) unwrapped continuous phase distribution (d) 3D rendering of the thickness profile of the microsphere (e) line profile of the thickness of microsphere obtained along the dashed line shown in (c).

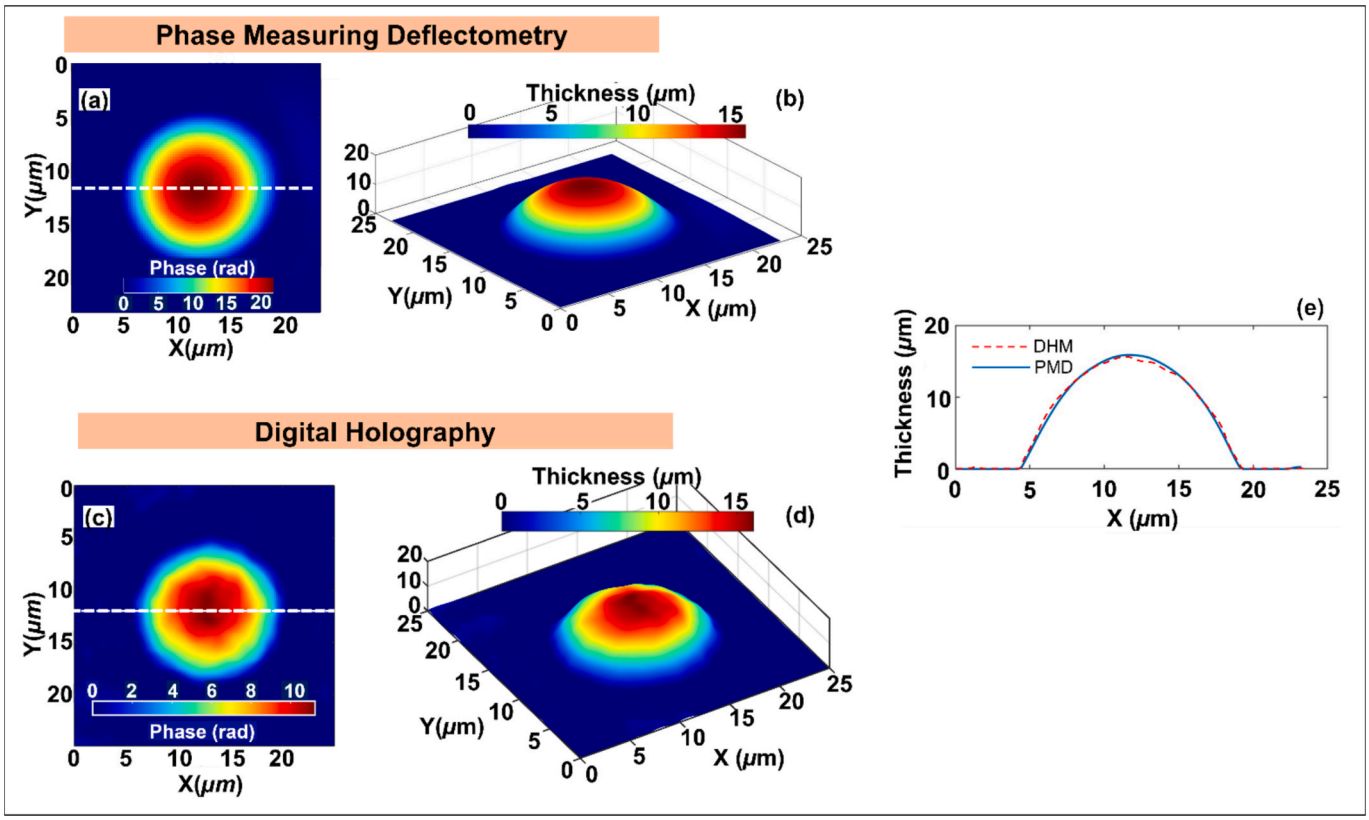

Fig. 6. Reconstruction of the transparent polystyrene microsphere of diameter 15 μm. Phase Measuring Deflectometry (a) unwrapped continuous phase distribution (b) 3D rendering of the thickness profile. Digital Holographic Microscopy-(c) continuous phase distribution (d) 3D rendering of the thickness profile. The thickness profile along the dashed lines is shown in Fig. 6a and c. Dashed line is the thickness profile obtained using DHM and the continuous line represents the thickness profile obtained using PMD.

processing the obtained phase maps. This phase stability (longitudinal measurement accuracy) is comparable to the phase stability obtained in DHM using a laser source [16]. The use of a laser source in DHM results in laser speckle noise and parasitic reflections, which may affect the longitudinal accuracy. On the other hand, the presented PMD technique uses a completely incoherent source in the form of a display screen, which can avoid such coherent noises. It should be noted that the DHM systems operate on the principle of interference, relying on optical setups involving beam splitters, lasers, and other precise opto-mechanical components. Since it is an interferometric technique, it provides high sensitivity to optical path length changes, which also makes the system susceptible to external factors such as vibrations and environmental noise. These challenges can restrict the use of DHM in rugged conditions. Additionally, in cases involving large optical path length changes, DHM systems may encounter fringe discontinuities leading to abrupt phase jumps or errors. While these challenges do not undermine the inherent advantages of DHM, alternative methods such as the one presented here, can address such issues by allowing flexible control over fringe density on the display screen. This flexibility makes PMD a practical choice in environments where large path length variations occur.

The presented microscope operates on the principle of measuring the deflection in the fringe pattern caused by the slope of the optical thickness (or changes in optical thickness). Like other cumulative measurement techniques, such as digital holography, the proposed system integrates the optical thickness along the viewing direction. Consequently, any changes in optical thickness above or below the observed plane are integrated to produce the resultant measurement. As a result, while the proposed system can measure the optical thickness of both plano-concave and biconcave objects, it may not be able to distinguish their exact shapes due to the cumulative nature of the measurement as in the case in digital holography. A tomographic approach would be required to accurately determine the true three-dimensional shape of the object. This could involve capturing projections from multiple directions, either by rotating the object or by adjusting the pattern and imaging system relative to the object.

After validating the technique's efficiency in shape visualization and thickness measurement, the proposed system was employed for imaging RBC and quantifying its thickness (Fig. 7). A thin smear of blood to achieve sparse RBC distribution was prepared on a microscope slide and imaged using the proposed PMD based microscope. Fig. 7(a) shows the continuous phase distribution, Fig. 7(b) represents the three-dimensional rendering of thickness distribution using refractive indices of red blood cell and that of blood plasma (medium in which the red blood cell is immersed) [14]. Fig. 7(c) depicts the line profile of the thickness along the line shown in Fig. 7(a). It can be seen from Fig. 7 that the technique is equally capable of shape visualization and the thickness measurement of biological cells.

5. Conclusion

We have demonstrated the effectiveness of PMD in microscopy for shape visualization and thickness measurement of transparent micro-objects such as transparent polystyrene microspheres and RBCs. PMD offers a cost-effective quantitative phase contrast imaging solution, using a smartphone screen, two microscope objective lenses, and a CCD array to produce results comparable to a digital holographic microscope. While DHM provides high-resolution phase maps and is well-suited for studying dynamic or live-cell phenomena, it typically requires a coherent laser source, precise interferometric alignment, and vibration isolation. In contrast, the proposed PMD-based system operates without a dedicated light source, uses incoherent illumination, has a simpler and

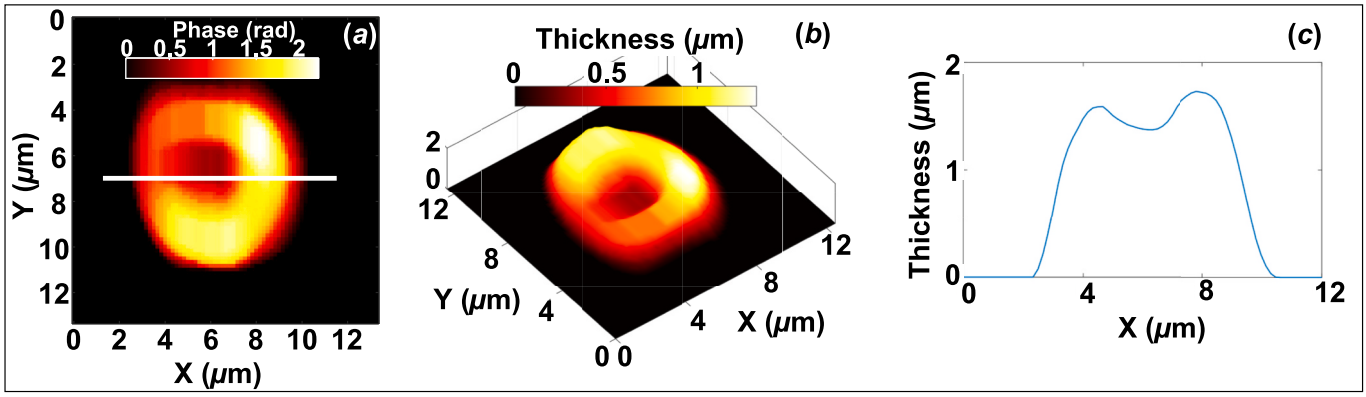

Fig. 7. Reconstruction of shape and line profile of the RBC using the scaling factor *K* obtained from the calibration process. (a) Unwrapped continuous phase distribution (b) 3D rendering of thickness distribution using the refractive index of red blood cell and blood plasma (c) line profile of thickness along the dashed line shown in (a). (For interpretation of the references to colour in this figure legend, the reader is referred to the web version of this article.)

more compact setup, and is inherently less sensitive to environmental disturbances. Additionally, PMD supports digital phase shifting without mechanical components, and its fringe density can be easily adjusted to tune sensitivity and measurement range.

The advantages of the proposed technique include the absence of a separate light source, a simple design, no need for vibrational isolation, digital phase shifting without mechanical movement, and adjustable fringe density for varied range and sensitivity in shape profiling and thickness measurement. It should be noted that by increasing the fringe density, the finer structures of the object could be measured. However, increasing the sensitivity of the measurement system could lead to a reduced range of measurement as even a small optical thickness variation will lead to the shift of one complete fringe, after which the phase values get repeated, limiting the measurement range. So, selecting a particular fringe density will depend on the dimensions (especially thickness) of the sample under investigation. The statement regarding the relationship between fringe density, measurement sensitivity, and measurement range is based on theoretical understanding and previous experiences with similar systems.

The technique maps the thickness profiles of transparent phase objects using a calibration constant *K*, obtained using known samples (5 μm diameter polystyrene microspheres). The calibration factor *K* can be affected by factors like tilting, perspective effects, or distortions in the imaging system, that can cause slight variations in the fringe pitch *p* across the field-of-view. The main aim of this manuscript is to present a proof-of-concept technique demonstrating the potential of PMD in the domain of phase contrast microscopy. This approach highlights the advantages of PMD, such as its immunity to environmental factors and its cost-effectiveness in developing a robust and inexpensive phase contrast microscope. For this proof-of-concept, a fixed scaling factor *K* was estimated for a particular geometry and orientation of the projected pattern, which remained the same throughout the measurements. Given the primary objective of introducing PMD as an alternative approach for phase contrast microscopy, a detailed investigation of variations in *K* lies beyond the scope of this study. However, future follow-up experiments will explore and analyze various parameters, including *K*, to enhance the accuracy and applicability of the technique. The experiments also used a broad-spectrum display that might introduce some wavelength-related effects. However, the objective of the study was to keep the system as raw and straightforward as possible. Refining the model to account for spectral effects, including potential wavelength dependence of *K*, will be an important step in future studies. These refinements could involve examining the impact of different wavelengths on phase accuracy and adjusting K accordingly. The present work assumes that the wavelength dependence of *K* is minimal, particularly given the scale of fringe variations relative to the size of the objects studied. Furthermore, future studies will also explore the influence of parameters like *p*, *d*, and wavelength on measurement accuracy.

Additionally, the use of a smartphone display to project fringe patterns introduces a practical limitation when higher-resolution imaging is desired. As the numerical aperture (NA) of the imaging lens increases, it begins to resolve the individual pixels of the display. This can lead to pixelation of the projected fringe patterns, causing deviations from the ideal sinusoidal profile and affecting phase measurement accuracy. Instead of a smoothly varying fringe pattern, the system may register pixelated or aliased patterns, limiting measurement precision. This effect becomes particularly significant when high fringe density is required to resolve fine structures, and must be considered carefully when designing high-NA or high-resolution PMD systems. Future versions of the system could explore higher-resolution displays or optical diffusion strategies to mitigate pixelation artifacts.

Since PMD has not been significantly exploited in the areas of biomedical imaging, we have attempted to present a proof-of-concept microscopy technique based on PMD using four-step phase shifting algorithms to visualize shape profiles and compute the thickness of transparent micro-objects. While the phase shifting algorithm has limitations in studying fast or dynamic phenomena, enhancing display refresh rates and synchronization with sensors can improve image acquisition speed and reduce operational duration. Various other phase extraction algorithms can also be explored that can work with low fringe density and contrast and a smaller number of fringe patterns to improve the robustness of the system. Moreover, utilizing machine learning algorithms can further improve the results, especially in the areas of cell identification and characterization, and disease diagnosis. Furthermore, efforts can be made to employ Fourier transform based fringe analysis algorithms to efficiently study dynamic phenomena.

For the proof-of-concept experiments presented in the manuscript, only sparse object distributions (only a few microscopes and blood cells in the field of view) were used and there are certain areas where efforts can be made to improve the quality of the results. It is also important to emphasize that the PMD technique is not proposed as a universal replacement for DHM but as a complementary approach for specific applications where its inherent robustness, simplicity, and cost-effectiveness offer significant advantages.

Live cell imaging is just one of the potential applications of the PMD-based system. Other potential applications include imaging transparent samples, inspecting microstructures, and analyzing heat flow or surface deformation in challenging environments.

This study highlights a novel adaptation of PMD beyond its conventional use in reflective surface metrology, demonstrating its feasibility for quantitative phase contrast imaging of transparent biological micro-objects. We believe this direction opens new possibilities for low-cost, compact imaging systems in biomedical research and diagnostics.

CRediT authorship contribution statement

Shivam Sharma: Writing – review & editing, Writing – original draft, Visualization, Validation, Software, Investigation, Formal analysis. **Vismay Trivedi:** Writing – review & editing, Writing – original draft, Visualization, Validation, Project administration, Investigation, Formal analysis, Conceptualization. **Swapnil Mahajan:** Visualization, Conceptualization. **Gyanendra Sheoran:** Writing – review & editing, Visualization. **Bahram Javidi:** Writing – review & editing, Visualization. **Arun Anand:** Writing – review & editing, Writing – original draft, Visualization, Validation, Supervision, Formal analysis, Conceptualization.

Funding

The work was supported by research grants from SERB (EMR/20 l7/002724), DAE-BRNS (2013/34/11/BRNS/504), DST-FIST, and DST-PURSE.

Declaration of competing interest

The authors declare that they have no known competing financial interests or personal relationships that could have appeared to influence the work reported in this paper.

Acknowledgements

Shivam Sharma would like to thank UGC for SRF. Vismay Trivedi would like to thank SERB for N-PDF.

Data availability

Data underlying the results presented in this letter are not publicly available at this time but may be obtained from the authors upon reasonable request.

References

[1] S. Suresh, Mechanical response of human red blood cells in health and disease: Some structure-property-function relationships, J. Mater. Res. 21 (2006) 1871–1877, https://doi.org/10.1557/jmr.2006.0260.
[2] D.B. Murphy, M.W. Davidson, Fundamentals of light microscopy and electronic imaging, Wiley (2012), https://doi.org/10.1002/9781118382905.
[3] N.M. Deshpande, S. Gite, R. Aluvalu, A review of microscopic analysis of blood cells for disease detection with AI perspective, PeerJ Comput. Sci. 7 (2021) e460.
[4] S. Kumar, D. Jiang, B. Sun, K.V. Seeley, J.W. Engle, Z. Sia, X. He, S. Neelamegham, W. Cai, J.F. Lovell, Labeling of erythrocytes by porphyrin-phospholipid, Adv. NanoBiomed Res. 1 (2021), https://doi.org/10.1002/anbr.202000013.
[5] A.S. Adewoyin, B. Nwogoh, Peripheral blood film - A review., Annals of Ibadan, Postgrad. Med. 12 (2014) 71–79.
[6] T.L. Nguyen, S. Pradeep, R.L. Judson-Torres, J. Reed, M.A. Teitell, T.A. Zangle, Quantitative phase imaging: Recent advances and expanding potential in biomedicine, ACS Nano 16 (2022) 11516–11544, https://doi.org/10.1021/acsnano.1c11507.
[7] U. Schnars, W. Jueptner, Digital holography, springer-verlag, Berlin/heidelberg (2005), https://doi.org/10.1007/b138284.
[8] T. Kreis, Handbook of Holographic Interferometry, Wiley (2004), https://doi.org/10.1002/3527604154.
[9] N.T. Shaked, M.T. Rinehart, A. Wax, Dual-interference-channel quantitative-phase microscopy of live cell dynamics, Opt. Lett. 34 (2009) 767, https://doi.org/10.1364/OL.34.000767.
[10] M.K. Kim, Digital Holographic Microscopy, in: Springer Series in Optical Sciences, 2011: pp. 149–190. Doi: 10.1007/978-1-4419-7793-9_11.
[11] M. Joglekar, V. Trivedi, R. Bhatt, V. Chhaniwal, S. Dubey, D. Claus, G. Pedrini, R. Leitgeb, B. Javidi, A. Anand, Compact, low cost, large field-of-view self-referencing digital holographic interference microscope, Optik (stuttg) 245 (2021) 167615, https://doi.org/10.1016/j.ijleo.2021.167615.
[12] N.T. Shaked, Quantitative phase microscopy of biological samples using a portable interferometer, Opt. Lett. 37 (2012) 2016, https://doi.org/10.1364/OL.37.002016.
[13] V. Trivedi, M. Joglekar, S. Mahajan, N. Patel, V. Chhaniwal, B. Javidi, A. Anand, Digital holographic imaging of refractive index distributions for defect detection, Opt. Laser Technol. 111 (2019) 439–446, https://doi.org/10.1016/j.optlastec.2018.10.024.
[14] S. Utadiya, V. Trivedi, K. Bhanderi, M. Joglekar, C. Limberkar, K. Patel, G. Sheoran, H. Cabrera, B. Javidi, A. Anand, Thickness and surface profiling of optically transparent and reflecting samples using lens-less self-referencing digital holographic microscopy, Appl. Surf. Sci. Adv. 18 (2023) 100484, https://doi.org/10.1016/j.apsadv.2023.100484.
[15] S. Utadiya, V. Trivedi, A. Srivastava, H. Cabrera, M.L. Crespo, G. Sheoran, A. Anand, Optical thickness measurement of occluded samples by lens-less Fourier transform digital holography, thermal loading, and machine learning, Appl. Opt. 63 (2024) B16, https://doi.org/10.1364/AO.503589.
[16] M. Joglekar, V. Trivedi, V. Chhaniwal, D. Claus, B. Javidi, A. Anand, LED based large field of view off-axis quantitative phase contrast microscopy by hologram multiplexing, Opt. Express 30 (2022) 29234, https://doi.org/10.1364/OE.444616.
[17] S. Mahajan, V. Trivedi, P. Vora, V. Chhaniwal, B. Javidi, A. Anand, Highly stable digital holographic microscope using Sagnac interferometer, Opt. Lett. 40 (2015) 3743, https://doi.org/10.1364/OL.40.003743.
[18] P. Vora, V. Trivedi, S. Mahajan, N. Patel, M. Joglekar, V. Chhaniwal, A.-R. Moradi, B. Javidi, A. Anand, Wide field of view common-path lateral-shearing digital holographic interference microscope, J. Biomed. Opt. 22 (2017) 1, https://doi.org/10.1117/1.JBO.22.12.126001.
[19] A. Anand, A. Faridian, V.K. Chhaniwal, S. Mahajan, V. Trivedi, S.K. Dubey, G. Pedrini, W. Osten, B. Javidi, Single beam Fourier transform digital holographic quantitative phase microscopy, Appl. Phys. Lett. 104 (2014) 103705, https://doi.org/10.1063/1.4868533.
[20] N. Patel, V. Trivedi, S. Mahajan, V. Chhaniwal, C. Fournier, S. Lee, B. Javidi, A. Anand, Wavefront division digital holographic microscopy, Biomed. Opt. Express 9 (2018) 2779, https://doi.org/10.1364/BOE.9.002779.
[21] S. Utadiya, V. Trivedi, G. Sheoran, A. Srivastava, D. Claus, H. Cabrera, A. Anand, Digital holographic imaging of thermal signatures and its use in inhomogeneity identification, Opt. Lasers Eng. 160 (2023) 107227, https://doi.org/10.1016/j.optlaseng.2022.107227.
[22] S. Utadiya, V. Trivedi, V. Singh, G. Sheoran, H. Cabrera, A. Srivastava, B. Javidi, A. Anand, Digital holographic characterization of multilayered structures by thermal scanning, Appl. Opt. 64 (2025) B134–B142, https://doi.org/10.1364/AO.545003.
[23] V. Trivedi, M. Joglekar, S. Utadiya, N. Chhiller, S. Sharma, G. Sheoran, A. Anand, Shape measurement of phase objects using fringe projection technique, in: P. Lehmann, W. Osten, A. Albertazzi Gonçalves (Eds.), Optical Measurement Systems for Industrial Inspection XIII, SPIE, 2023, p. 104, https://doi.org/10.1117/12.2673865.
[24] V.K. Chhaniwal, C.S. Narayanamurthy, A. Anand, Imaging of mass transfer process using artificial fringe deflection, Opt. Eng. 53 (2014) 074106, https://doi.org/10.1117/1.OE.53.7.074106.
[25] V. Trivedi, M. Joglekar, S. Mahajan, V. Chhaniwal, B. Javidi, A. Anand, Portable device based on beam deflection for refractive index mapping and diffusion coefficient measurement, Opt. Eng. 58 (2019) 1, https://doi.org/10.1117/1.OE.58.1.014101.
[26] H. Guo, H. Zhou, P.P. Banerjee, Use of structured light in 3D reconstruction of transparent objects, Appl. Opt. 61 (2022) B314, https://doi.org/10.1364/AO.444708.
[27] Y. Xu, F. Gao, X. Jiang, A brief review of the technological advancements of phase measuring deflectometry, PhotoniX 1 (2020) 14, https://doi.org/10.1186/s43074-020-00015-9.
[28] P.S. Huang, S. Zhang, Fast three-step phase-shifting algorithm, Appl. Opt. 45 (2006) 5086, https://doi.org/10.1364/AO.45.005086.
[29] Q. Kemao, Two-dimensional windowed Fourier transform for fringe pattern analysis: Principles, applications and implementations, Opt. Lasers Eng. 45 (2007) 304–317, https://doi.org/10.1016/j.optlaseng.2005.10.012.
[30] K. Samanta, J. Joseph, An overview of structured illumination microscopy: Recent advances and perspectives, J. Optics (united Kingdom) 23 (2021), https://doi.org/10.1088/2040-8986/ac3675.
[31] X. Chen, S. Zhong, Y. Hou, R. Cao, W. Wang, D. Li, Q. Dai, D. Kim, P. Xi, Superresolution structured illumination microscopy reconstruction algorithms: A review, Light Sci. Appl. 12 (2023), https://doi.org/10.1038/s41377-023-01204-4.
[32] K. Aflalo, P. Gao, V. Trivedi, A. Sanjeev, Z. Zalevsky, Optical super-resolution imaging: A review and perspective, Opt. Lasers Eng. 183 (2024) 108536, https://doi.org/10.1016/j.optlaseng.2024.108536.
[33] M. Born, E. Wolf, A.B. Bhatia, P.C. Clemmow, D. Gabor, A.R. Stokes, A.M. Taylor, P.A. Wayman, W.L. Wilcock, Principles of Optics, Cambridge University Press, 1999. Doi: 10.1017/CBO9781139644181.
[34] L. Huang, M. Idir, C. Zuo, A. Asundi, Review of phase measuring deflectometry, Opt. Lasers Eng. 107 (2018) 247–257, https://doi.org/10.1016/j.optlaseng.2018.03.026.
[35] S.S. Gorthi, P. Rastogi, Fringe projection techniques: Whither we are? Opt. Lasers Eng. 48 (2010) 133–140, https://doi.org/10.1016/j.optlaseng.2009.09.001.
[36] E. Zendejas-Hernández, G. Trujillo-Schiaffino, M. Anguiano-Morales, D.P. Salas-Peimbert, L.F. Corral-Martínez, N. Tornero-Martínez, Spatial and temporal methods for fringe pattern analysis: A review, J. Opt. 52 (2023) 888–899, https://doi.org/10.1007/s12596-023-01166-1.
[37] M. Takeda, K. Mutoh, Fourier transform profilometry for the automatic measurement of 3-D object shapes, Appl. Opt. 22 (1983) 3977, https://doi.org/10.1364/AO.22.003977.
[38] J. Schwiegerling, Optical Specification, Fabrication, and Testing (2015), https://doi.org/10.1117/3.1002794.
[39] C. Zuo, S. Feng, L. Huang, T. Tao, W. Yin, Q. Chen, Phase shifting algorithms for fringe projection profilometry: A review, Opt. Lasers Eng. 109 (2018), https://doi.org/10.1016/j.optlaseng.2018.04.019.

[40] J.L. Flores, B. Bravo-Medina, J.A. Ferrari, One-frame two-dimensional deflectometry for phase retrieval by addition of orthogonal fringe patterns, Appl. Opt. 52 (2013) 6537, https://doi.org/10.1364/AO.52.006537.
[41] M.A. Herráez, D.R. Burton, M.J. Lalor, M.A. Gdeisat, Fast two-dimensional phase-unwrapping algorithm based on sorting by reliability following a noncontinuous path, Appl. Opt. 41 (2002) 7437, https://doi.org/10.1364/AO.41.007437.
[42] A. Anand, I. Moon, B. Javidi, Automated Disease Identification With 3-D Optical Imaging: A Medical Diagnostic Tool, Proceedings of the IEEE 105 (2017) 924–946. Doi: 10.1109/JPROC.2016.2636238.